


ARTICLE

Open Access

Molecular basis for hierarchical histone de- β -hydroxybutyrylation by SIRT3

Xingrun Zhang¹, Ruili Cao¹, Jinrong Niu¹, Shumin Yang¹, Huida Ma¹, Shuai Zhao¹ and Haitao Li¹ 

Abstract

Chemical modifications on histones constitute a key mechanism for gene regulation in chromatin context. Recently, histone lysine β -hydroxybutyrylation (Kbhb) was identified as a new form of histone acylation that connects starvation-responsive metabolism to epigenetic regulation. Sirtuins are a family of NAD⁺-dependent deacetylases. Through systematic profiling studies, we show that human SIRT3 displays class-selective histone de- β -hydroxybutyrylase activities with preference for H3 K4, K9, K18, K23, K27, and H4K16, but not for H4 K5, K8, K12, which distinguishes it from the Zn-dependent HDACs. Structural studies revealed a hydrogen bond-lined hydrophobic pocket favored for the S-form Kbhb recognition and catalysis. β -backbone but not side chain-mediated interactions around Kbhb dominate sequence motif recognition, explaining the broad site-specificity of SIRT3. The observed class-selectivity of SIRT3 is due to an entropically unfavorable barrier associated with the glycine-flanking motif that the histone Kbhb resides in. Collectively, we reveal the molecular basis for class-selective histone de- β -hydroxybutyrylation by SIRT3, shedding lights on the function of sirtuins in Kbhb biology through hierarchical deacylation.

Introduction

Posttranslational modifications (PTMs) on histones, often installed, recognized, and removed by their cognate “writers, readers, and erasers” in a type-specific and site-specific manner, play critical roles in regulating diverse chromatin-templated cellular processes^{1,2}. Histone lysine acetylation (Kac) was firstly identified in early 1960s³, possessing a primary function in regulating gene transcription^{4,5}. Extensive studies on the dynamic regulation and selective recognition of histone Kac have elucidated its role in various cellular regulatory mechanisms^{6,7}. Aided by advanced mass spectrometry-based proteomics technologies, a cornucopia of non-acetyl histone acylations have been identified, such as formylation (fo)⁸, propionylation (pr), butyrylation (bu)^{9,10}, crotonoylation (cr)¹¹, succinylation (succ)¹², glutarylation (glu)¹³, 2-hydroxyisobutyrylation (hib)¹⁴, and β -hydroxybutyrylation (bhb)¹⁵. Identification

of writers, readers, and erasers of these acyl marks are important to further elucidate the chromatin signaling pathways in which they are involved^{16,17}.

Histone lysine β -hydroxybutyrylation (Kbhb) has been detected in yeast, fly, mouse and human, and 44 Kbhb sites have been identified in human and mouse cells¹⁵. β -hydroxybutyrylation modified on the ϵ -group of lysine distinguishes itself from acetylation by its branch, chiral, and four-carbon length properties. The levels of histone Kbhb are significantly elevated under the conditions of starvation or streptozotocin-induced diabetic ketosis. It has been proposed that histone Kbhb directly connects ketone body metabolism to gene regulation, given the high concentration of β -hydroxybutyrate in blood during fasting, starvation, or prolonged intense exercise^{15,18}. Importantly, histone H3K9bhb is associated with gene upregulation in a starvation-responsive manner, and distinguishes an amount of these genes from others that are marked by H3K9ac and H3K4me3, suggesting a unique role in connecting epigenetic regulation and starvation-responsive metabolism¹⁵. To further elucidate Kbhb

Correspondence: Haitao Li (lht@tsinghua.edu.cn)

¹MOE Key Laboratory of Protein Sciences, Beijing Advanced Innovation Center for Structural Biology, Beijing Frontier Research Center for Biological Structure, Tsinghua-Peking Joint Center for Life Sciences, Department of Basic Medical Sciences, School of Medicine, Tsinghua University, 100084 Beijing, China

© The Author(s) 2019



Open Access This article is licensed under a Creative Commons Attribution 4.0 International License, which permits use, sharing, adaptation, distribution and reproduction in any medium or format, as long as you give appropriate credit to the original author(s) and the source, provide a link to the Creative Commons license, and indicate if changes were made. The images or other third party material in this article are included in the article's Creative Commons license, unless indicated otherwise in a credit line to the material. If material is not included in the article's Creative Commons license and your intended use is not permitted by statutory regulation or exceeds the permitted use, you will need to obtain permission directly from the copyright holder. To view a copy of this license, visit <http://creativecommons.org/licenses/by/4.0/>.

functions in gene regulation, its cognate eraser(s) awaits to be characterized.

The sirtuin family proteins (e.g., human SIRT1-7), a class of NAD⁺-dependent deacetylases that remove acetyl marks from various cellular proteins including histones, function in a wide range of biological pathways in responses to nutritional and environmental perturbations¹⁹. Activation of sirtuins increases the lifespan of several model organisms, while mutation or inhibition of sirtuins leads to the onset of aging phenotypes^{20,21}. Recently, emerging evidence suggested that sirtuins could remove acyl groups other than acetyl from lysine residues²². For example, SIRT1-3 can remove crotonyl marks from lysine²³, while SIRT4 is reported to have deglutaryl- and dehydroxymethyl-glutarylation activities^{24,25}. SIRT5 removes the malonyl, succinyl, and glutaryl marks^{13,26,27}. SIRT6 preferentially hydrolyzes long alkyl acyl marks from lysines, such as myristoyl mark²⁸. In summary, sirtuins play an important role in removing various acyl marks from lysines of histone as well as non-histone substrates.

SIRT3 is a predominant mitochondria matrix protein that modulates the activity of key metabolic enzymes via protein deacetylation²⁹. Besides, several studies reported that SIRT3 could act as a histone deacetylase both in vitro and in vivo^{23,30–32}, suggesting a moonlighting function of SIRT3 in nucleus³³. Through systematic profiling studies, here we reported that human SIRT3 functions as a histone de- β -hydroxybutyrylase at sites H3 K4, K9, K18, K23, K27, and H4K16. Interestingly, SIRT3 is incapable of removing bhb at sites H4 K5, K8, K12 that have flanking glycine residues both in vitro and in cells. Such class-selectivity is not observed in HDAC3, a key member of the Zn-dependent histone deacetylases. Co-crystal structural analyses of SIRT3 bound to H3K9bhb, H3K4bhb, and H4K16bhb peptides as well as structural-based mutagenesis studies revealed the molecular basis underlying class-selective recognition and erasure of histone Kbh. Hence, our work on hierarchical histone deacylation by SIRT3 suggests a potential regulatory mechanism that links acylation dynamics to gene regulation under metabolic alternations.

Results

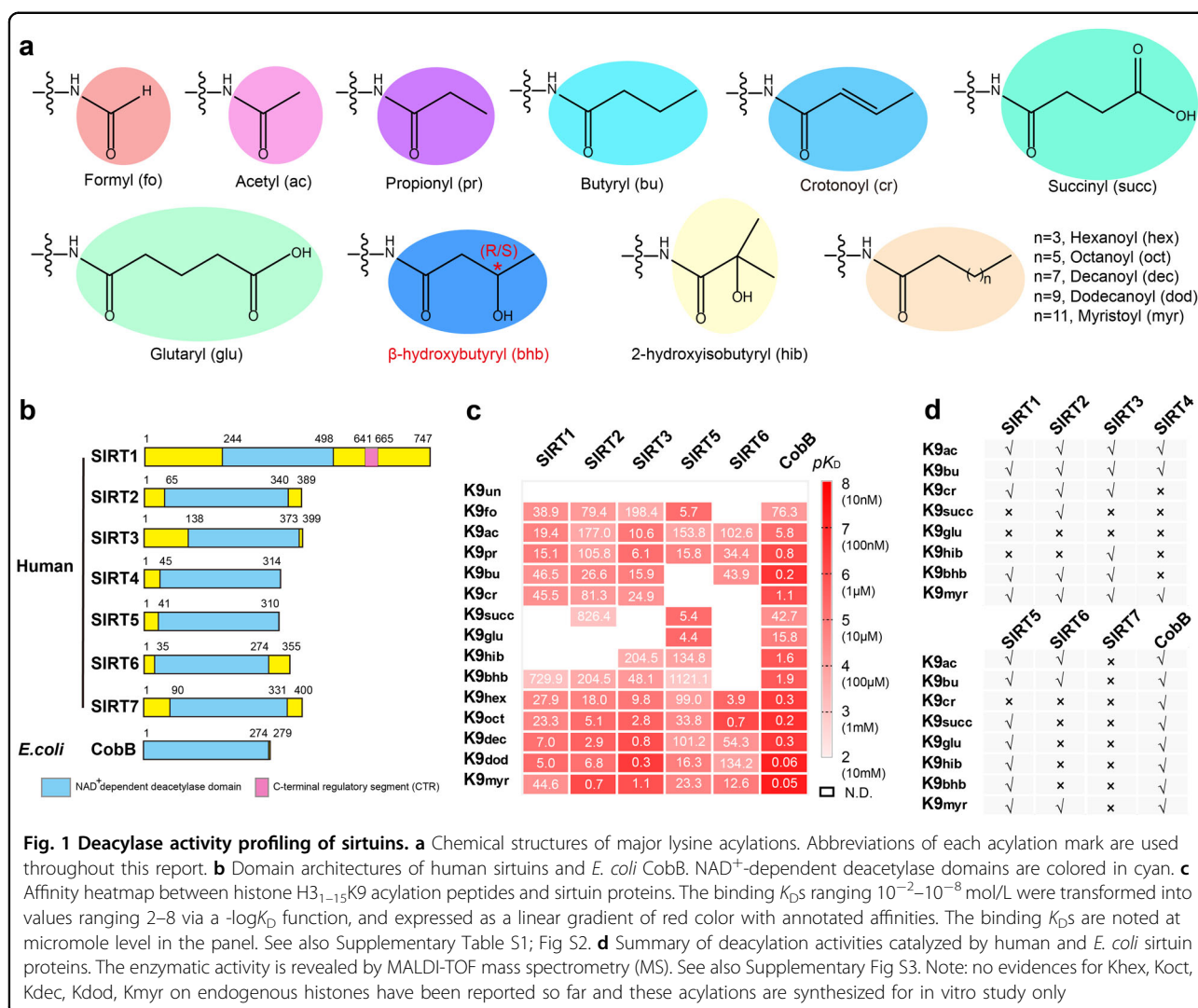
Systematic profiling histone deacetylase activities of sirtuins

By means of click chemistry followed by affinity purification and competition assays, Bao et al revealed that SIRT3 is a histone decrotonylase and binds to H3K4 crotonylation (H3K4cr) peptide substrate at an affinity of $\sim 25.1 \mu\text{M}$ in the absence of NAD⁺. Taking histone H3K9 acylation as a probe, we synthesized a panel of histone H3 peptides encompassing residues 1–15 (H3_{1–15}) with lysine 9 bearing acetyl and thirteen other non-acetyl acyl marks

(Fig. 1a). Next, we expressed and purified NAD⁺-dependent deacetylase domains of all human sirtuins as well as full-length bacteria CobB that serves as a prototype sirtuin control (Fig. 1b and Supplementary Fig. S1). We then performed isothermal titration calorimetry (ITC) to profile interactions between the well-behaved sirtuin proteins (SIRT1-3, 5, 6, and CobB) and histone H3K9 acylation peptides in the absence of NAD⁺. The yields of SIRT4 and SIRT7 were low and thereby were not used for ITC titration.

On the binding affinity heatmap of ninety interaction pairs, each sirtuin family member displays unique H3K9 acylation binding feature (Fig. 1c and Supplementary Fig. S2; Table S1). Previously reported specific deacetylase activities of sirtuins are all corroborated by micromolar binding affinities in this heatmap, with K_D values of $24.9 \mu\text{M}$ for SIRT3-Kcr, of 5.4 and $4.4 \mu\text{M}$ for SIRT5-Ksucc and SIRT5-Kglu, and of $12.6 \mu\text{M}$ for SIRT6-Kmyr (Fig. 1c)^{13,23,26,28}. Most sirtuins bind well to straight-chain acyl marks from 1-carbon Kfo to 14-carbon Kmyr, except that SIRT5 does not bind Kbu/Kcr, and SIRT6 does not bind Kfo/Kcr. The two acidic acyl marks, namely Kglu and Ksucc, are recognized by SIRT5 and CobB; interestingly, Ksucc but not Kglu is accommodated by SIRT2. The hydroxyl-replaced Khib and Kbh. marks are both recognized by SIRT3, SIRT5, and CobB; however, only Kbh. but not Khib can be recognized by SIRT1 and SIRT2 (Fig. 1c). The diversified acyllysine selectivity reflects delicate design of the active center over a common sirtuin scaffold. It is interesting to note that most sirtuins displayed optimal binding towards non-acetyl acyl marks, notably those with longer alkyl chain (Fig. 1c and Supplementary Fig. S2; Table S1).

Next, we measured deacetylase activities of all sirtuins including SIRT4 and SIRT7 by mass spectrometry (MS) against eight H3K9 acylation marks: Kac, Kbu, Kcr, Ksucc, Kglu, Khib, Kbh., and Kmyr. In general, all binding events mentioned above were well translated into deacetylase activities (Fig. 1d and Supplementary Fig. S3). This is consistent with the notion that sirtuin enzymes preferentially bind to acylated peptide first before NAD⁺ loading³⁴, and efficient peptide substrate engagement is required for deacylation to occur. Collectively, bacterial CobB is able to deacylate eight H3K9 acylation marks tested but SIRT7 does none of them. SIRT4 and SIRT6 are able to hydrolyze Kac, Kbu, and Kmyr but not the acidic Ksucc/Kglu, the hydroxyl-replaced Khib/Kbh., and the rigidified Kcr marks. In contrast, SIRT5 is able to remove most marks except for Kcr. SIRT1-3 behave similarly and are sensitive to acidic Ksucc/Kglu, except for SIRT2-Ksucc; additionally, SIRT1 and SIRT2 cannot hydrolyze Khib, while SIRT3 displays a deacetylase activity towards both Khib and Kbh. (Fig. 1d).

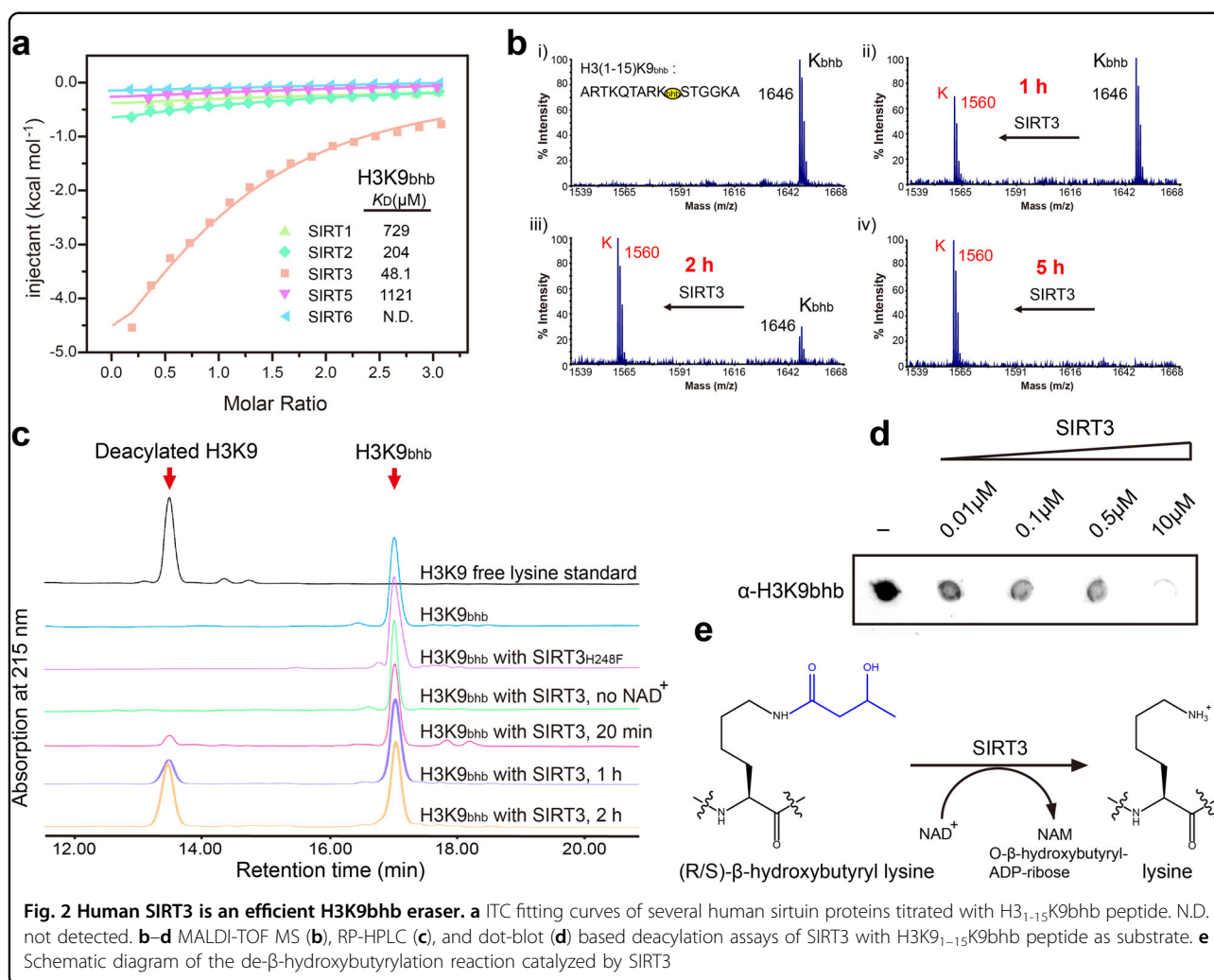


Enzymatic characterization of SIRT3 as an H3K9bhb eraser

Since SIRT3 showed strongest affinity for H3K9bhb among human sirtuins (SIRT3, $K_D = 48.1 \mu\text{M}$; SIRT1, $K_D = 729 \mu\text{M}$; SIRT2, $K_D = 204 \mu\text{M}$; SIRT5, $K_D = 1121 \mu\text{M}$; SIRT6, N.D.) (Fig. 2a), and SIRT4 and SIRT7 displayed no enzymatic activity towards H3K9bhb (Fig. 1d), we next chose SIRT3 for in-depth enzymatic and structural characterizations. MS, RP-HPLC (reverse-phase high performance liquid chromatography) and dot-blot-based assays were used to probe the H3K9bhb deacetylase activity of SIRT3 (Fig. 2b–d). As expected, SIRT3 removes the bhb group from H3K9bhb in a time, enzyme-dose, and NAD⁺ cofactor dependent manner, demonstrating an NAD⁺-dependent de- β -hydroxybutyrylation activity (Fig. 2e). Mutation of residue H248 (H248F) that is critical for the catalysis of deacetylation by SIRT3 completely abolished its de- β -hydroxybutyrylation activity (Fig. 2c), indicating that SIRT3 catalyzes K_{bhb} hydrolysis by a similar mechanism as it does for K_{ac}³⁵.

Overall structure of SIRT3 bound to H3K9bhb peptide

To decipher the structural basis underlying H3K9bhb recognition by SIRT3, we determined the binary crystal structure of SIRT3_{118–399} bound to the H3_{6–15}K9bhb peptide in an NAD⁺ free state at 1.95 Å resolution (Supplementary Table S2). There is one SIRT3 monomer in one crystallographic asymmetric unit. Based on the electron density, we could model residues 122–395 of SIRT3 and trace the “₇ARKSTGG₁₃” segment of the H3 peptide (Fig. 3a). SIRT3 adopts a classical sirtuin fold that consists of a zinc-binding small lobe and a NAD⁺-binding large lobe arranged in a Rossmann fold (Fig. 3b). The histone peptide (and NAD⁺) binds to a cleft formed at the interface of the two lobes. Structural alignment of the binary complex with an apo form SIRT3 (PDB: 3GLS) revealed induced bending of the small lobe upon H3K9bhb peptide insertion (Fig. 3c), consistent with previous report³⁵. We calculated a rotation angle of 18.6° based on the DynDom3D webserver analysis³⁶. The



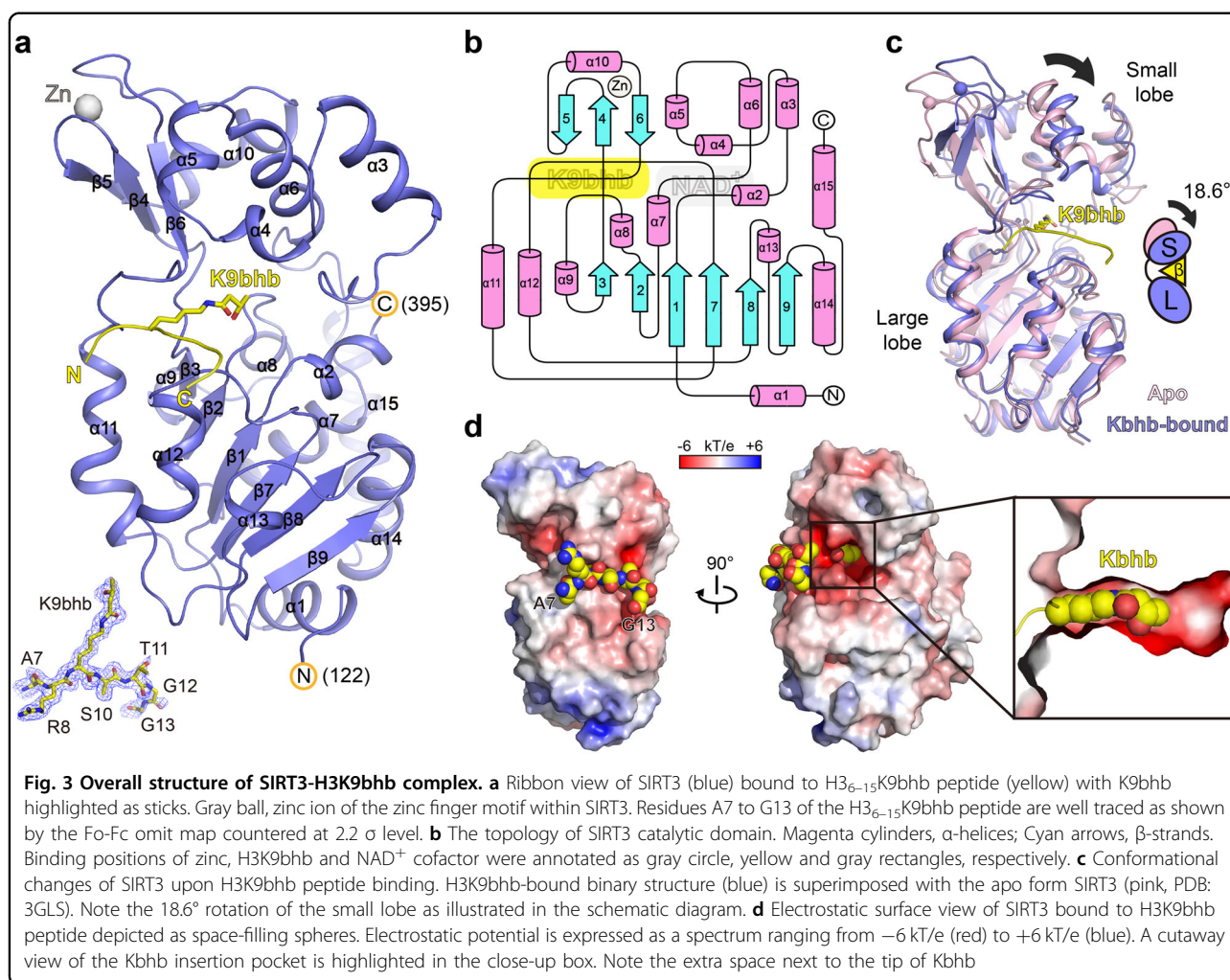
peptide-binding surface is largely negatively charged, being electrostatically favorable for the basic histone peptide targeting (Fig. 3d, left). There is a snug fitting of the H3K9bhb peptide into the substrate-binding pocket with Kbhb side chain inserted into an elongated tunnel (Fig. 3d, right). Consistent with the observed preference of SIRT3 for long-chain acylations, extra space exists next to the bhb group, being well positioned to accommodate long-chain acyl marks like Kdod and Kdec (Fig. 1c).

Interaction details for H3K9bhb recognition by SIRT3

In the binary structure of SIRT3 bound to H3K9bhb, the backbone of H3 segment "A7-R8-K9-S10-T11" engages five hydrogen bonding pairs, including A7(CO):L298(NH), K9(NH):E296(CO), K9(CO):G295(NH) from the upper side and S10(NH):E325(CO), S10(CO):E325(NH) from lower side (Fig. 4a, b). These are further strengthened by additional H3 side-chain mediated hydrogen bonds involving R8:G295 (upper) and T11:E323 (lower) (Fig. 4a, b).

The Kbhb mark is inserted into an elongated pocket formed by residues F294, V292, F180, I230, Q228, H248, and V324 (Fig. 4c). Besides an effect of charge neutralization of lysine, the bhb moiety of Kbhb affords extra hydrophobicity and hydrogen-bond forming capacity. Compliantly, the Kbhb mark is recognized by both hydrophobic contacts involving residues F294, V324, F180, I230, and hydrogen bonding interactions involving residues Q228, H248, V292 and a molecule of water (Fig. 4c). SIRT3 can deacylate both Kbhb and Kcr marks. As revealed in previous structural studies²³, the π - π stacking between F180 and Kcr plane as well as hydrophobic contacts contribute to Kcr recognition (Fig. 4dii). The saturated bhb moiety cannot form π - π stacking with F180. As an adaptation, hydrophobic contacts with F180 and I230, as well as direct hydrogen bonds of the β -hydroxyl group with H248 and Q228 contribute to bhb-specific mode of recognition (Fig. 4di).

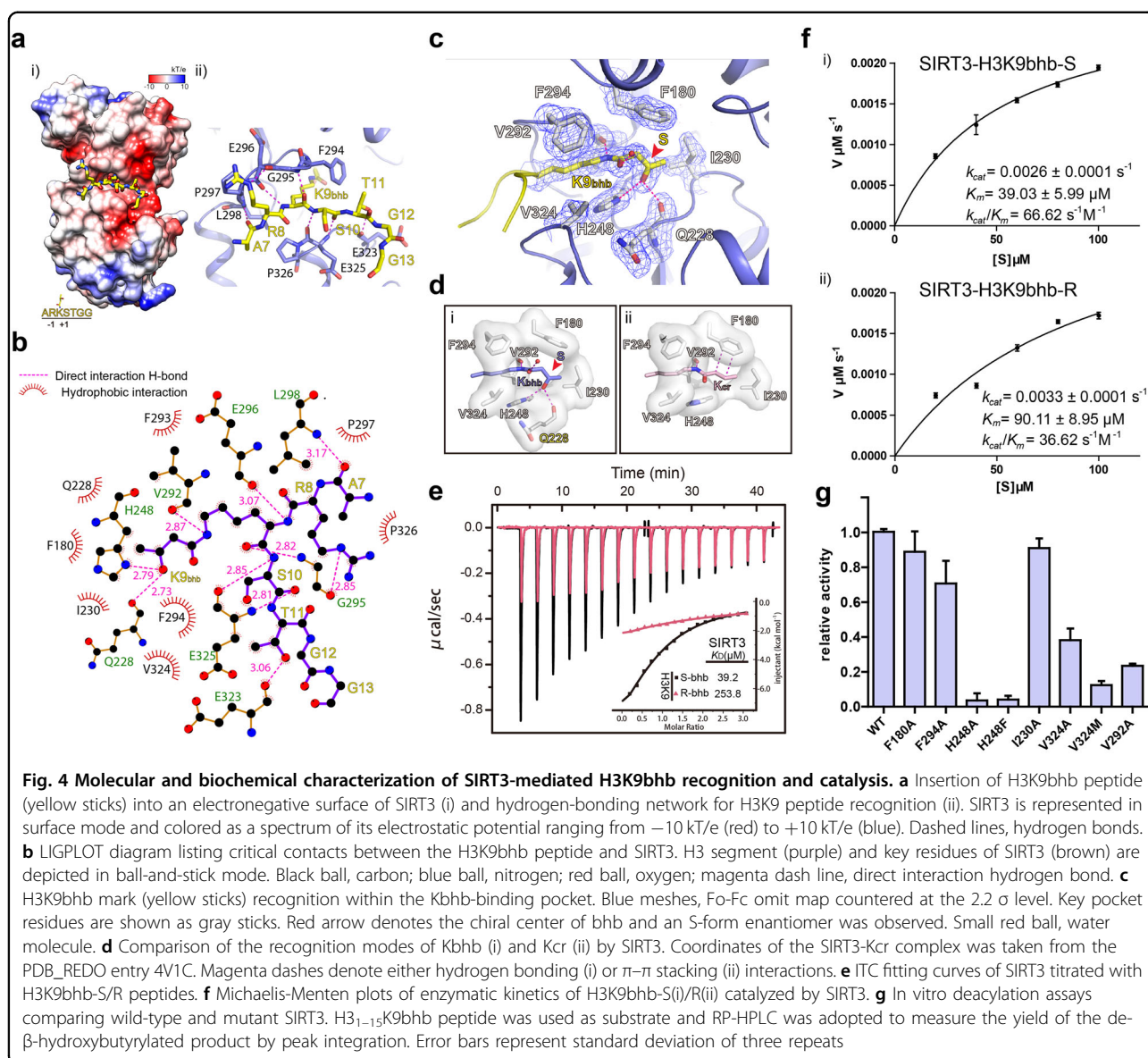
It has not escaped our attention that both electron density (Fig. 4c) and interaction environment (Fig. 4di)



clearly suggest that the S-form enantiomer of bhb is captured in the crystal structure despite the fact that the Kbhb peptide was synthesized as the R/S racemic mixture. In support, ITC titration using newly synthesized stereospecific H3K9bhb peptides revealed a ~6.5-fold binding preference for S-bhb ($K_D = 39.2 \mu\text{M}$) over R-bhb ($K_D = 253.8 \mu\text{M}$) (Fig. 4e). Consistently, enzymatic kinetic assays revealed a K_m of 39.03 μM for S-bhb and a K_m of 90.11 μM for R-bhb, and in total ~2-fold catalytic efficiency preference for the S-form ($k_{\text{cat}}/K_m = 66.62 \text{ s}^{-1} \text{ M}^{-1}$) over the R-form ($k_{\text{cat}}/K_m = 36.62 \text{ s}^{-1} \text{ M}^{-1}$) enantiomers (Fig. 4f). Our structural analyses revealed that the S-form bhb is concurrently stabilized by hydrogen bonding and hydrophobic contacts. By contrast, in the case of R-form Kbhb, the substrate engagement mode is imperfect since the abovementioned hydrogen bonding interactions and the hydrophobic contacts are not compatible (Supplementary Fig. S4a).

Catalytic center and mutagenesis-based enzymatic studies

In order to validate the functional importance of the pocket residues, we generated corresponding mutants of SIRT3₁₁₈₋₃₉₉ and measured their deacetylase activity by RP-HPLC. As shown in Fig. 4g, mutation of the catalytic residue H248 (H248A and H248F) almost completely abrogated the activity, attesting to its essential role in catalysis and/or substrate recognition. F180A, I230A, V292A, F294A, and V324A are also detrimental to the hydrolysis of Kbhb by SIRT3 to various degrees. We designed another mutant, residue V324M, intended for blocking insertion of the Kbhb moiety into its binding pocket. This mutant, retaining only about 15% activity of the wild-type enzyme, is most severe in inhibiting the hydrolysis of Kbhb by SIRT3 besides the H248 mutants (Fig. 4g). The V324M mutant is about 14-fold lower in binding affinity with K9bhb than wild-type SIRT3 (SIRT3_{WT}-H3K9_{bhb}, $K_D = 48.1 \mu\text{M}$; SIRT3_{V324M}-

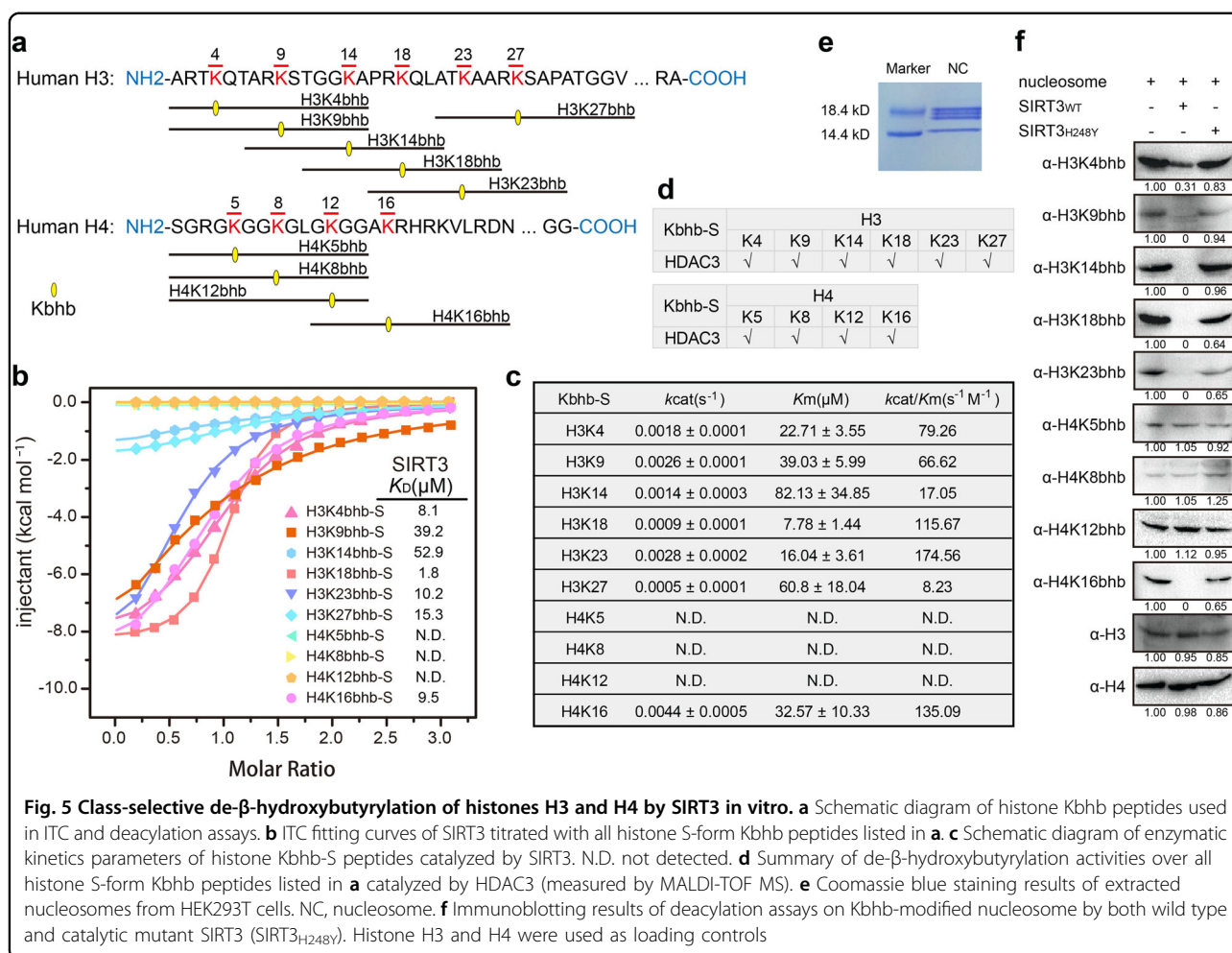


H3K9_{bhb}, $K_D = 664 \mu\text{M}$) possibly due to the blocking of Kbhb insertion into the binding pocket as we designed (Supplementary Fig. S4b). These results demonstrate the important roles of these residues in recognition and hydrolysis of Kbhb by SIRT3.

Kbhb site-selectivity of SIRT3 over H3 and H4 N-terminal tails in vitro

To investigate the site-selectivity for recognition and hydrolysis of Kbhb by SIRT3, we tested whether SIRT3 can engage and remove bhb mark on well-known acylation sites of histones, including K4, K9, K14, K18, K23, K27 of H3, and K5, K8, K12, K16 of H4 (Fig. 5a). In ITC assays, SIRT3 broadly binds to Kbhb mark with affinities $8.1 \mu\text{M}$ for H3K4bhb, $39.2 \mu\text{M}$ for H3K9bhb, $52.9 \mu\text{M}$ for

H3K14bhb, $1.8 \mu\text{M}$ for H3K18bhb, $10.2 \mu\text{M}$ for H3K23bhb, $15.3 \mu\text{M}$ for H3K27bhb, and $9.5 \mu\text{M}$ for H4K16bhb in the S-form (Fig. 5b), which displayed ~ 2.3 to 7.6-fold binding preference over the R-form (Supplementary Fig. S5a). By contrast, SIRT3 does not bind to K5bhb, K8bhb, and K12bhb of H4 in both chiral forms, and thus displays a unique class-selectivity against these sites. Consistently, we observed broad de- β -hydroxybutyrylase activities of SIRT3 on tested histone sites other than H4 K5, K8, and K12 in RP-HPLC based deacylation assays (Fig. 5c and Supplementary Figs. S5b, S6). The enzymatic kinetics results show a relatively broad range of k_{cat}/K_m ($79.26 \text{ s}^{-1} \text{ M}^{-1}$ for H3K4bhb-S, $66.62 \text{ s}^{-1} \text{ M}^{-1}$ for H3K9bhb-S, $17.05 \text{ s}^{-1} \text{ M}^{-1}$ for H3K14bhb-S, $115.67 \text{ s}^{-1} \text{ M}^{-1}$ for H3K18bhb-S,



$174.56 s^{-1} M^{-1}$ for H3K23bhb-S, $8.23 s^{-1} M^{-1}$ for H3K27bhb-S, and $135.09 s^{-1} M^{-1}$ for H4K16bhb-S), which is consistent with ITC binding assays. The glycine-flanking motifs shared by H4K5bhb (GKGG), K8bhb (GGKG), and K12bhb (GKGG) probably account for the enzymatic incompetence of SIRT3. In support, H3K14bhb that has two flanking glycine residues from the N-terminus (GGKA) displayed weakest binding affinity (Fig. 5b and Supplementary Fig. S5a). In comparison to SIRT3, the class I Zn-dependent histone deacetylase HDAC3 showed no class-selectivity on histone H3 and H4 tails (Fig. 5d and Supplementary Figs. S5b, S7), highlighting a molecular functional distinction between the two subfamilies of histone deacylases.

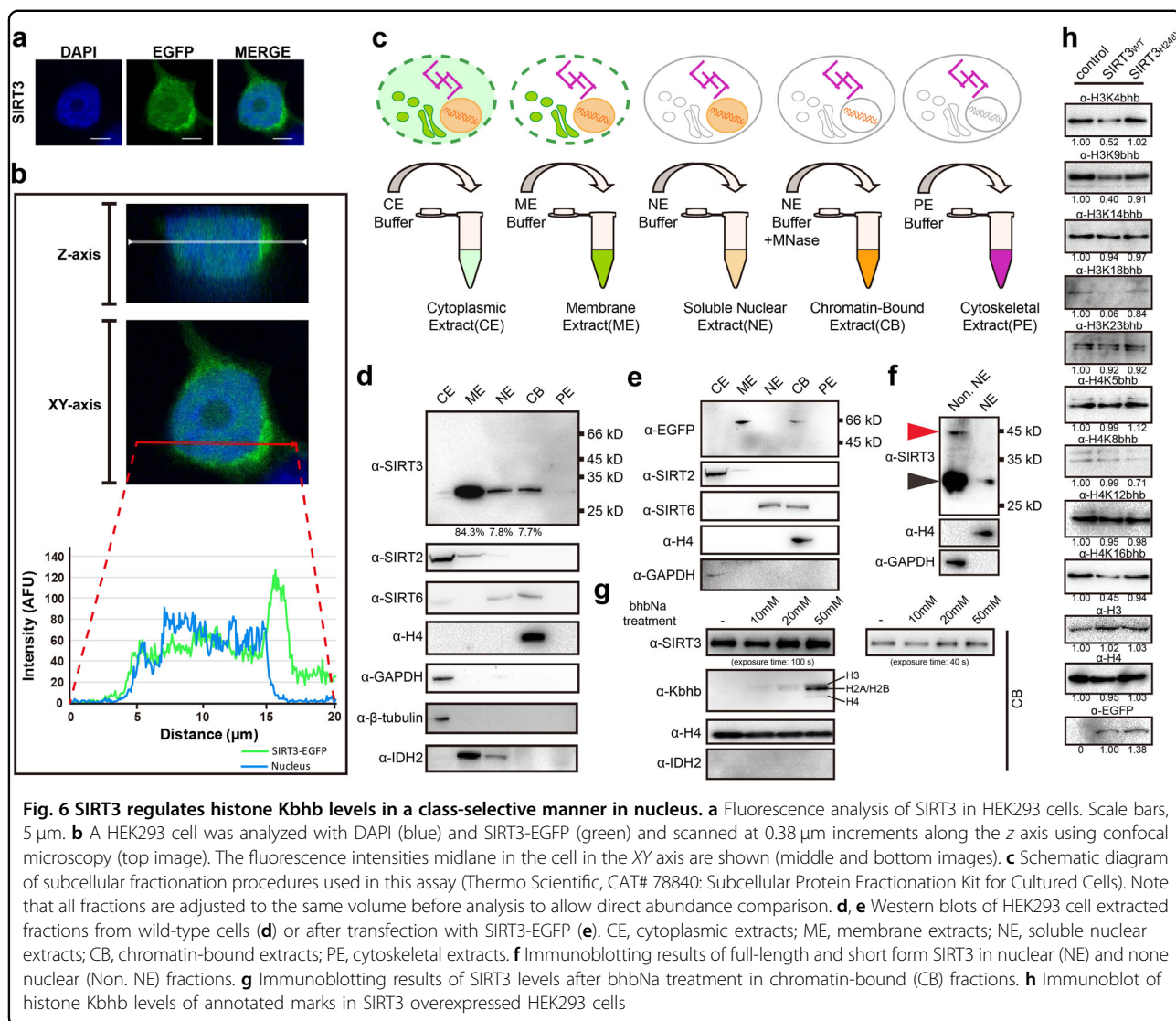
To test if SIRT3 could deacylate Kbhb at nucleosomal level, we prepared Kbhb modified nucleosomes from bhb-treated HEK293 cell and subjected them for deacylation by SIRT3. Dot blot assays verified the site-selectivity and type-selectivity of corresponding antibodies (Supplementary Fig. S8). After SIRT3 treatment, we immunoblotted Kbhb of the SDS-PAGE resolved histone samples (Fig.

5e). We were able to detect clear deacylation activity of SIRT3 over H3K4bhb, H3K9bhb, H3K14bhb, H3K18bhb, H3K23bhb, and H4K16bhb, but not H4K5bhb, H4K8bhb, and H4K12bhb (Fig. 5f). Importantly, an active site mutant of SIRT3, H248Y, displayed no activity toward Kbhb-modified nucleosomes, suggesting a direct role of SIRT3 in nucleosomal deacylation of Kbhb.

Collectively, the above data demonstrate a class-selective de-β-hydroxybutyrylation activity of SIRT3 that distinguishes it from HDACs at both peptide and nucleosome levels in vitro.

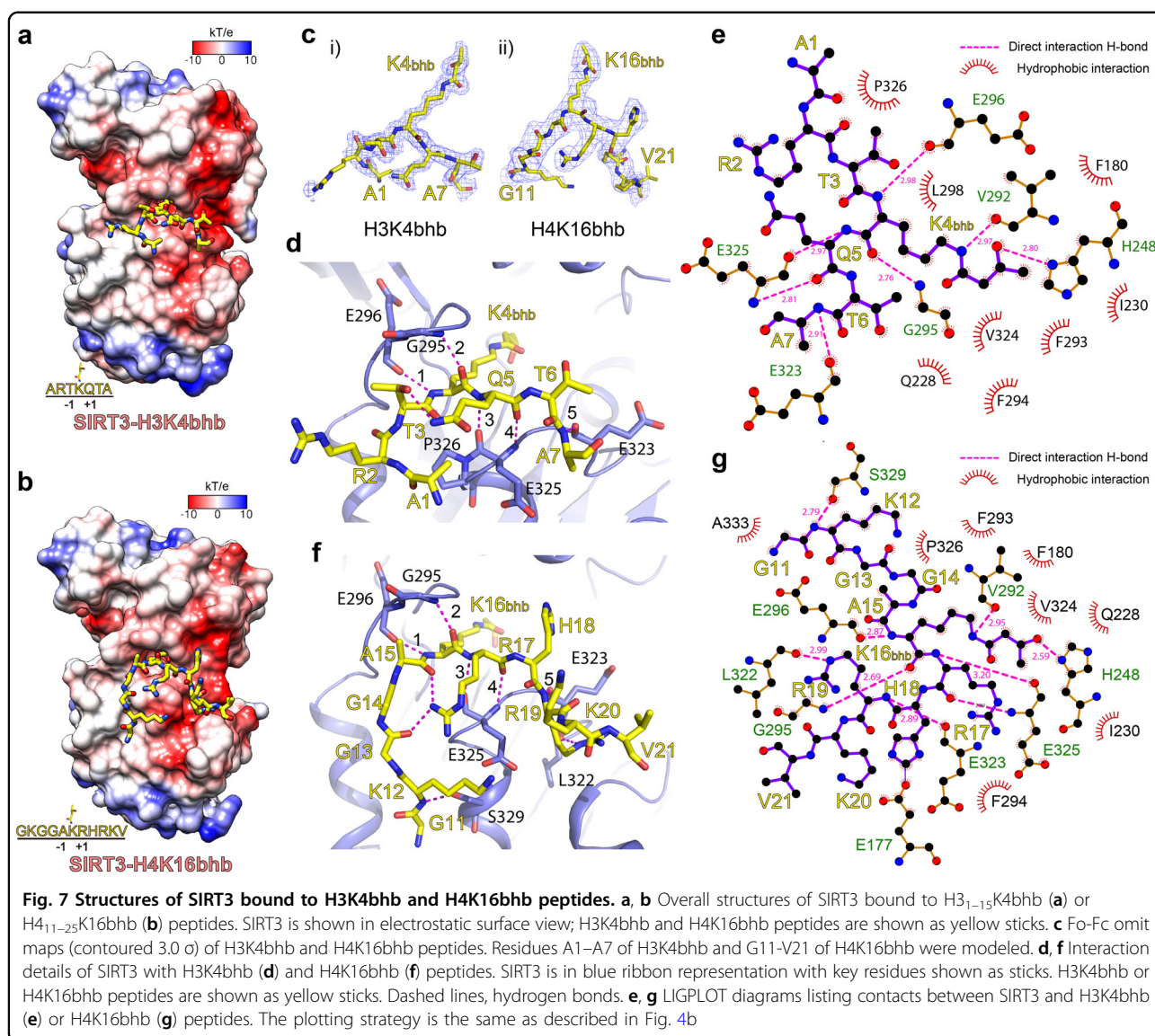
SIRT3 regulates histone Kbhb levels in nucleus

SIRT3 is mainly a mitochondria matrix protein that regulates metabolism biochemically via protein deacetylation²⁹. To confirm its nuclear presence, we performed fluorescence-based co-localization and cell fractionation studies in HEK293 cells. Z-stack 3D imaging of C-terminally EGFP-labeled SIRT3 revealed clear fluorescence signals in nucleus despite much brighter signals in mitochondria (Fig. 6a, b and Supplementary Fig. S9,



Movies S1, S2). Subcellular fractionation assays showed that overexpressed or endogenous SIRT3 could be detected in both mitochondria and nuclear fractions (Fig. 6c–f). Notably, ~10% of total SIRT3 was observed in the chromatin-bound extraction. Immunoblotting assays using bbbNa treated cells showed that SIRT3 can be recruited onto chromatin in a dosage-dependent manner, possibly induced by upregulated histone Kbbh levels (Fig. 6g). Interestingly, while the Kbbh signal is enriched on histone H3 under lower and more physiological bbbNa concentrations (10 and 20 mM), the Kbbh levels of H2A/H2B are preferentially upregulated at a supplemented bbbNa concentration of 50 mM (Fig. 6g), suggesting mechanisms of histone type-specific Kbbh regulation in response to metabolic alternations. Collectively, all the above results suggest a direct association of SIRT3 with chromatin.

We further checked the deacylation activity in cells with overexpressed SIRT3. Consistently, overexpression of wild type but not the H248Y mutant SIRT3 reduced bbb levels at sites H3K4, H3K9, H3K18 and H4K16, but not H4K5, H4K8, H4K12 (Fig. 6h). Interestingly, the levels of H3K14bbb and H3K23bbb are not influenced at cellular level upon SIRT3 overexpression (Fig. 6h), which contradicts with a clear nucleosomal substrate activity in vitro (Fig. 5f), and suggests possible mechanisms of active establishment of H3K14bbb and H3K23bbb patterns in HEK293 cells. Of note, a “reading-and-writing” cross-talk between H3K14 and H3K23 acylations have been implicated in the case of MOZ/MORF (a.k.a. KAT6A/6B) complexes that are responsible for maintaining global histone H3K23ac level in a BRPF1-dependent manner³⁷. We have previously shown that the DPF domains of MOZ and DPF2 are specific histone H3K14 acylation readers,



and bind to H3K14bhb (racemic mixture) at 110 μ M and 0.93 μ M, respectively³⁸.

Recognitions of H3K4bhb and H4K16bhb by SIRT3

To compare consensus and difference in distinct histone Kbhb site recognition by SIRT3, we next solved the binary structures of SIRT3 bound to H3₁₋₁₅K4bhb and H4₁₁₋₂₅K16bhb peptides at 1.9 Å and 2.9 Å , respectively (Supplementary Table S2). Both H3K4bhb and H4K16bhb peptides are stapled into an acidic surface of SIRT3 with well-traced electron densities (Fig. 7a–c). The H3K4bhb peptide adopts the same orientation as that of H3K9bhb and the segment “A1-R2-T3-K4bhb-Q5-T6-A7” was modeled (Fig. 7d). Multiple hydrogen bonds and hydrophobic contacts contribute to H3K4bhb-SIRT3 interaction with the Kbhb mark recognized essentially the same

way as K9bhb (Fig. 7e). In particular, H3K4bhb backbone engages five sets of hydrogen bonds, including K4_(NH):E296_(CO), K4_(CO):G295_(NH) from the upper side and Q5_(NH):E325_(CO), Q5_(CO):E325_(NH), A7_(NH):E323_(CO) from lower side (Fig. 7d, e). We also observed an intra-chain hydrogen bond between T3 and Q5 side chains, which may stabilize a bending conformation of the peptide backbone and thus facilitate H3K4bhb recognition.

The H4K16bhb peptide is recognized in a similar manner as H3K4bhb, which is through five sets of backbone-mediated hydrogen bonds and extensive hydrophobic contacts (Fig. 7f, g). Besides, H4K16bhb binding is further strengthened by two unique hydrogen bonding pairs involving distal flanking residues K12 (K12: S329) and R19 (R19:L322), as well as intra-chain hydrogen bonds involving R17 (R17:G13 and R17:A15) (Fig. 7f, g).

These extra hydrogen-bonding interactions explained the relatively high binding affinity (H3K4bhb, $K_D = 8.1 \mu\text{M}$; H4K16bhb, $K_D = 9.5 \mu\text{M}$) compared with H3K9bhb recognition.

Molecular basis underlying class-selectivity of SIRT3

Next, we aligned all three binary SIRT3 structures reported in this study, and found that four pairs of backbone interactions involving residues E296, G295, and E325 are highly conserved, which serves as a common binding mode and dominates Kbhb sequence motif recognition (Fig. 8a). Dihedral angle analysis revealed that main-chain geometries of the central Kbhb motif ($X_iK_iX_{i+1}$) fall in the core β -strand region with proper ϕ/ψ dihedral angle distribution (Fig. 8a)³⁹. Interestingly, those sites that SIRT3 is incapable or inefficient to catalyze are characteristic of a glycine-flanking feature (Fig. 5a). Although the poor tolerance cannot be due to steric clash since glycine is side-chain free, the high degree of rotational freedom endowed by glycine could create an entropically unfavorable barrier for the abovementioned backbone interactions, thereby explaining the observed class-selectivity of SIRT3. In support, calorimetric titrations revealed a high entropy cost of $-28.1 \text{ cal/mol/deg}$ for H3K14bhb, which is in sharp contrast with an entropy change of -4.2 cal/mol/deg for H3K4bhb and -7.8 cal/mol/deg for H4K16bhb (Supplementary Table S1). Conceivably, the bending conformations of peptide substrate are pre-stabilized in part by intra-chain hydrogen bonding interactions in the cases of H3K4bhb and H4K16bhb (Fig. 7d, f).

Previous structural studies of HDAC1 (a close paralog of HDAC3) bound to an H4K16ac peptide analog suggested that class I HDACs adopt a deep and narrow pocket for acetylysine insertion, and the histone peptide is organized in a “turn-staple” conformation around an acidic residue (D99 of HDAC1) for backbone engagement (Fig. 8b)⁴⁰. Both SIRT3 and class I HDACs primarily rely on the substrate backbone for recognition, accounting for their relatively broad site-specificity. In the meantime, the backbone-binding mode of class I HDACs is not β -conformation selective, which is distinct from SIRT3 and therefore explains the observed non class-selectivity of HDAC3.

To further verify our analysis, we synthesized a series of mutant histone peptides by introducing or removing Kbhb-flanking glycine residues around representative sites including H3K4, H3K9, H3K14, H3K18, H4K8, H4K16 and subjected them for binding and enzymatic assays using SIRT3 (Fig. 8c). As summarized in Fig. 8d, single G mutation around H3K4bhb caused reduced binding by 15-fold for T3G ($K_D = 205.3 \mu\text{M}$) and by five-fold for Q5G ($K_D = 79.4 \mu\text{M}$), while “T3GQ5G” double mutation completely disrupted binding. Similarly, the

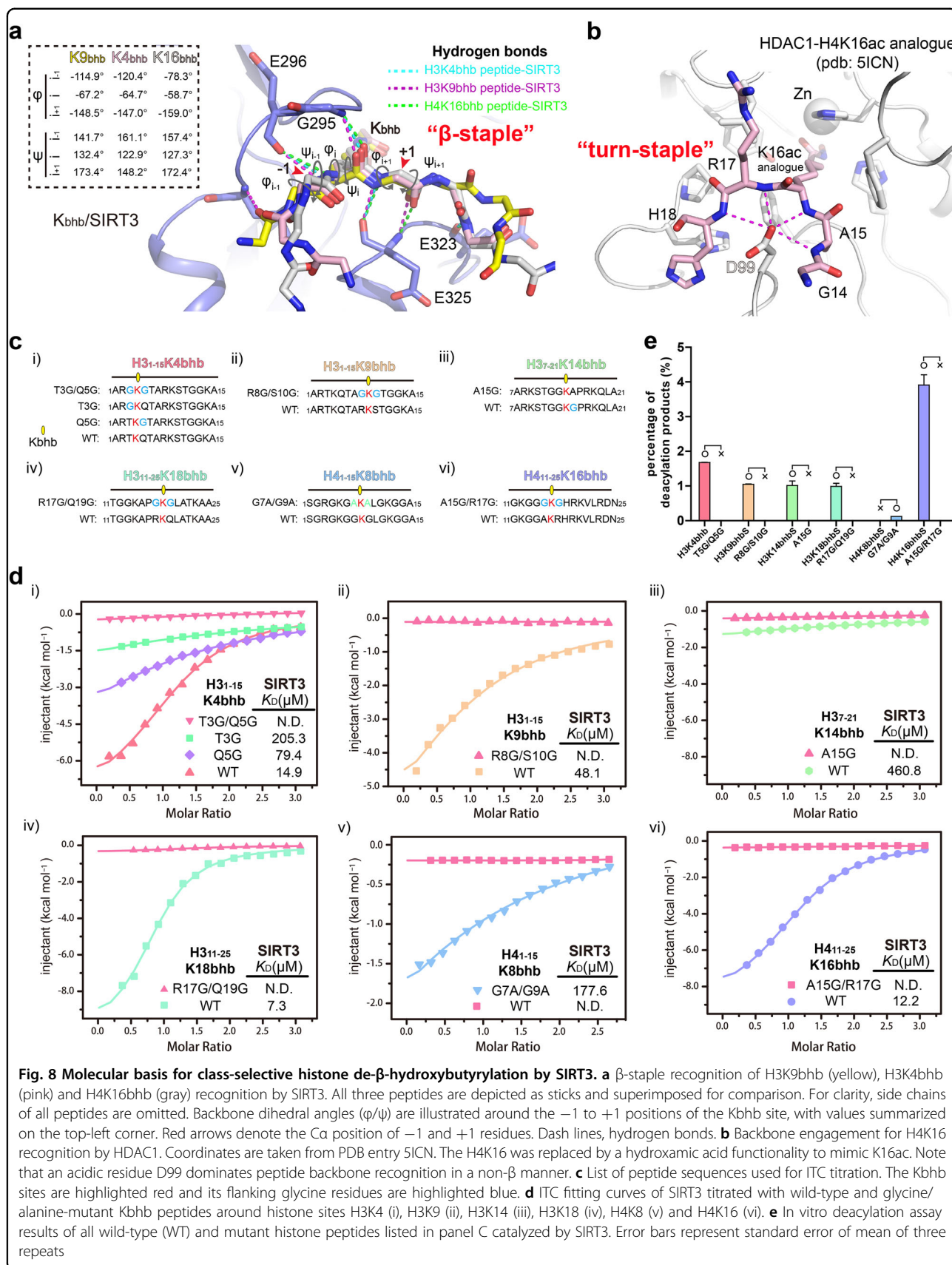
existence of two Kbhb-flanking glycine residues at sites H3K9 (R8G/S10G), H3K14 (A15G), H3K18 (R17G/Q19G), and H4K16 (A15G/R17G) abolish interaction completely. In further support, reverse “G-to-A” mutation in the case of H4(G7A/G9A)K8bhb restored binding to a K_D of $177.6 \mu\text{M}$ (Fig. 8d). The results of enzymatic assays are consistent with our ITC binding assay results. All “GG” mutant peptides cannot be catalyzed by SIRT3, while “G-to-A” mutation in H4(G7A/G9A)K8bhb peptide rescues its deacylation ability by SIRT3 (Fig. 8e). Moreover, successful restoration of binding and catalysis by “G-to-A” mutation suggests that lack of charge/polarity in the “GG” motifs is unlikely an alternative reason for their being weak SIRT3 substrates.

Overall, our structural, binding and enzymatic studies demonstrate the molecular basis for anti-selective deacylation of glycine-flanking Kbhb sites of histones by SIRT3.

Discussion

A large collection of non-acetyl acylations has been identified on histone lysines, posing new challenges to characterize the cognate regulators and regulatory mechanisms^{16,41}. Lysine β -hydroxybutyrylation is unique as it possesses a hydroxyl-group and is chiral and structurally branched in nature (Fig. 1a). Through profiling studies, here we demonstrate that four human sirtuins (SIRT1-3, SIRT5), bacterial sirtuin CobB, and HDAC3 are able to catalyze the hydrolysis of histone Kbhb. Such newly identified de- β -hydroxybutyrylase activities broaden the landscape of histone PTMs that are regulated by sirtuins as well as class I HDACs. Importantly, the observed class-selectivity of SIRT3 but not HDAC3 provides new insights into a regulatory mechanism that histone Kbhb as well as other histone acylations likely involves through hierarchical histone deacylation by sirtuins.

Our structural studies revealed a hydrogen bond-lined hydrophobic pocket of SIRT3 for Kbhb recognition and catalysis. The recognition mode of Kbhb is different from that of Kcr (Fig. 4d). Besides a common hydrogen bond between V292 and the amide NH of Kbhb/Kcr, the bhb group is uniquely stabilized by hydrogen bonding of its β -hydroxyl with Q228 and H248 of SIRT3; additionally, F180 and I230 contribute to critical hydrophobic contacts with the hydrocarbon portion of bhb. Intriguingly, what is captured in the crystal structure is the S-form bhb, whose stereo configuration best permits the observed hydrophobic contact (Fig. 4c). Such a stereo-selectivity may have interesting functional implications given the fact that the R- β -hydroxybutyrate is the primary form of ketone body, while the S-form bhb-CoA is mainly converted from trans-cr-CoA via a hydration reaction especially during the short-chain fatty acids (SCFA) metabolism^{42,43}. The prevalence of Kbhb stereo-specific modification and its



regulation in cell remains to be explored in future studies. Our profiling studies also showed that another hydroxyl-substituted acyllysine, Khib, could be recognized and hydrolyzed by SIRT3, SIRT5, and CobB, but not SIRT1 and SIRT2 (Fig. 1a, c, d). The conservation and divergence of Khib versus Kbhb recognition by different sirtuin family members awaits further structural elucidations.

SIRT3 displayed both broad site-specificity (recognizing multiple acylation sites) and strict class-selectivity (unable to recognize a group of acylation sites) in histone de- β -hydroxybutyrylation. At the molecular level, these seemingly conflicting properties are well explained by a consensus β -staple selectivity of SIRT3⁴⁴. As revealed by our parallel structural analyses, we showed that SIRT3 selects against glycine-flanking motifs due to their intrinsic flexibility. In addition to sites of H4K5, H4K8, H4K12 investigated here, other Kbhb sites of similar motifs are expected resistant to SIRT3 deacylation as well. As a key regulator in mitochondria, SIRT3-sensitive mitochondrial acetylome has been profiled^{45,46}. Remarkably, the “ β -staple rule” is also conserved, in which flanking glycine or proline residues that are detrimental to the β -structure are disfavored^{47,48}. Given the sequence and structural similarities of human sirtuins (Supplementary Fig. S10), the observed backbone selectivity is likely conserved among different sirtuin members or of different acylation types. This is supported by previous biochemical profiling studies using either acetyl-peptide microarray⁴⁶ or pre-acylated (Kbhb, Khib not included) designer nucleosome library^{49,50}, in which glycine-flanking Kac peptides or acylated H4 tail were shown to be poor substrates for all human sirtuins. HDAC3 also possesses histone de- β -hydroxybutyrylation activities but displays no clear class selectivity, likely because the Zn-dependent HDACs do not require a β -staple conformation of peptidyl substrate for recognition⁵¹.

Histone acetyl as well as non-acetyl acylations are often linked to active gene transcription. Intriguingly, the establishment of histone acetyl/acylation states are likely hierarchical, which is reflected by the fact that many histone acetyl/acyl-transferases are often organized into large complexes that contain histone acylation reader modules⁵². For example, our recent work on YEATS2-containing ATAC acetyltransferase complex revealed a “read-write” Kac signal amplification mechanism in which recognition of H3K27ac by YEATS2 is required for ATAC-dependent maintenance of H3K9ac, thus ensuring full activation of ribosomal genes through establishment of histone hyperacetylation⁵³. Here we revealed that downregulation of histone acylation levels by sirtuin family members are also hierarchical, indicative of a mechanism of hierarchical gene repression. Conceivably, those acylation sites that survive sirtuin treatment may serve as cis-acting marks to avoid unwanted chromatin

compaction; on the other hand, they may act as seeds for re-establishment of a hyper-acylation pattern for gene reactivation by recruiting downstream effector complexes. Such a mechanism is supported by the existence of glycine-flanking motif-specific readers, such as the Brdt bromodomain that recognizes H4 K5acK8ac acetylation patterns^{54,55}.

In summary, we demonstrate that the sirtuin family member SIRT3 is an eraser of Kbhb with class-selectivity against non- β (e.g., glycine-flanking) sequence motifs. Our work on hierarchical histone deacylation by SIRT3 suggests a potential regulatory mechanism that connects metabolism to gene regulation through dynamic acylations in sirtuin and modification biology.

Materials and methods

Protein and peptide preparation

Human sirtuin genes are kind gifts from Dr. Jiahuai Han at Xiamen University. The NAD⁺-dependent deacetylase domain encompassing residues 118–399 of SIRT3 was subcloned into a pSUMOH10 vector (modified based on pET28b) containing an N-terminal 10xHIS-SUMO tag. All the mutants of SIRT3 were generated by the QuickChange site-directed mutagenesis strategy and verified by sequencing. Wild-type SIRT3_{118–399} was overexpressed in the *Escherichia coli* BL21 (DE3) strain (Novagen). After induction with 0.2 mM isopropyl β -D-thiogalactoside (IPTG) at 16 °C in LB medium supplemented with 0.1 mM ZnCl₂ overnight, cells were harvested by centrifugation and suspended in buffer A (500 mM NaCl, 20 mM Tris-HCl, pH 7.5, 5% glycerol, 20 mM imidazole), then disrupted by an EmulsiFlex-C3 homogenizer (Avestin). The lysate was further cleared by centrifugation, and the supernatant was loaded onto a HisTrap affinity column. After buffer A washing, bound proteins were subjected to on-column cleavage by ULP1 SUMO protease. The tag-free SIRT3_{118–399} protein was collected as flow-through, centrifuge-concentrated, and then purified by an anion-exchange QHP column followed by size exclusion chromatography on a Superdex 75 column (GE Healthcare). Purified peak fractions were pooled, concentrated, aliquoted, and stored at –80 °C for future use. All mutant SIRT3 and other sirtuin family proteins were purified using essentially the same procedure as described above.

All the histone peptides used in this study were synthesized at >95% purity by Beijing SciLight Biotechnology Ltd. Co.

Isothermal titration calorimetry

Experiments were performed at 25 °C on a MicroCal PEAQ-ITC instrument (Malvern Instruments). The sample cell containing 200 μ L of 50 μ M protein was titrated with 17 successive injections of 750 μ M peptide.

Acquired titration curves were fitted with the Origin 7.0 program using the “one set of binding sites” binding model. Protein concentrations were measured based on the UV absorption at 280 nm. Peptide concentrations were measured by weighing in large quantity.

In vitro deacylation assays

For deacylation activity profiling studies, the reaction system was prepared by mixing 5 µg of each sirtuin, 1 µg of each acylated lysine peptide and 5 mM NAD⁺ in a buffer solution containing 20 mM Tris-HCl, pH 7.5 and 1 mM DTT. For SIRT3 catalyzed deacylation assays, 1 µM SIRT3 and 100 µM of each histone Kbbh peptide were added into the same reaction solution. For enzymatic kinetics studies, 1 µM of SIRT3 was incubated with different concentrations of histone H3_{1–15}K9bbh-S/R (20, 40, 60, 80, 100, 200, 300, 400, and 500 µM) in the same reaction buffer at 37 °C for a certain period of time within the initial linear range. After incubation, the reactions were stopped by adding trifluoroacetic acid (TFA) to a final concentration of 5% (v/v) followed by immediate frozen in liquid nitrogen. Enzyme-free reaction systems were used as controls. The resultant reaction mixtures were then analyzed either RP-HPLC or MALDI-TOF MS.

For RP-HPLC analysis, samples were analyzed by a Dionex/Thermo UltiMate 3000 HPLC system with an AcclaimTM RSLC 120 C18 column (2.1 mm × 100 mm, 2.2 µm). After loading, the reaction mixtures were washed by buffer A (0.1% TFA in water) for 10 min, and then eluted by a gradient of 1–20% buffer B (0.1% TFA in acetonitrile) over 20 min. The flow rate was 0.4 mL/min, and the wavelength for UV detection was 215 nm. For mass spectrometry, samples were analyzed by a 4800 plus MALDI TOF/TOF Analyzer (Applied Biosystems/MDS SCIEX) and operated in the Reflector Positive mode using 4000 Series Explorer Software. Laser intensity was set up to 3500 V.

For dot-blot deacylation experiment, 500 ng histone peptide H3_{1–15}K9bbh was firstly added to nitrocellulose (NC) membrane, which is then air-dried and incubated with SIRT3-containing solution for 2 h at 37 °C. SIRT3 were prepared as a concentration gradient (0, 0.01, 0.05, 0.1, 0.5, and 10 µM) in reaction buffer 100 mM NaCl, 20 mM Tris-HCl, pH 7.5, 1 mM DTT, and 5 mM NAD⁺. After reaction, anti-H3K9bbh antibody (PTM Biolabs) was used to monitor the residue H3K9bbh on the membrane.

For nucleosome-based de-β-hydroxybutyrylation assays, Kbbh-modified nucleosomes were prepared using bbb-treated HEK293T cells, and then are subjected for SIRT3 treatment. The reaction system was prepared by mixing 1 µg/µL wild type SIRT3 or its catalytic mutant H248Y, 1 µg/µL extracted nucleosomes and 5 mM NAD⁺ in a buffer solution containing 20 mM Tris-HCl, pH 7.5,

350 mM NaCl and 1 mM DTT. After incubation at 37 °C for 1 h, the reaction was stopped by adding 5× loading buffer, then boiled at 100 °C for 10 min. Enzyme-free reaction systems were used as controls. The resultant reaction mixtures were then analyzed by immunoblotting assays.

Crystallization, data collection, and structure determination

Crystallization was performed via the sitting drop vapor diffusion method under 18 °C by mixing 1 µL protein with 1 µL reservoir solution. Wild-type SIRT3_{118–399} (8.7 mg/mL) was premixed with H3_{6–15}K9bbh, H3_{1–15}K4bbh, or H4_{11–25}K16bbh peptide in a 1:20 molar ratio in buffer 100 mM NaCl, 20 mM Tris-HCl, pH 7.5, and 2 mM DTT. Complex crystals were obtained in the reservoir solutions 0.1 M MES pH 6.5, 25% PEG 1000 for SIRT3-H3_{6–15}K9bbh, 0.2 M Li₂SO₄, 0.1 M sodium citrate, pH 6.0, 19% PEG 3350 for SIRT3-H3_{1–15}K4bbh, and 0.1 M Bicine, pH 9.0, 10% PEG 6000 for SIRT3-H4_{11–25}K16bbh, respectively.

For data collection, crystals were flash-frozen in liquid nitrogen under cryoprotectant solutions, which are corresponding reservoir solutions supplemented with 10% glycerol for SIRT3-H3_{1–15}K4bbh and SIRT3-H3_{6–15}K9bbh, and 25% ethylene glycol for SIRT3-H4_{11–25}K16bbh. Diffraction data were collected at beamline BL17U1 at Shanghai Synchrotron Radiation Facility at 0.9792 Å. The diffraction data were indexed, integrated, and merged using the HKL2000 software package⁵⁶. The complex structures were solved by molecular replacement using Molrep⁵⁷ from the CCP4 suite with the H3K4cr-bound SIRT3 structure (PDB: 4V1C) as the search model. Refinement and model building were performed with PHENIX⁵⁸ and COOT⁵⁹, respectively. The data collection and structure refinement statistics are summarized in Table S2.

Immunoblotting

HEK293T cells were collected and boiled in RIPA lysis buffer (ThermoFisher) in the presence of NAM, TSA, and protease inhibitor cocktail (Selleck). Proteins in the lysate were then separated by SDS-PAGE and transferred onto a NC membrane for blotting using annotated anti-Kbbh or anti-histone antibodies (PTM Biolabs). A dilution factor of 1:2000 was used for most primary antibodies. The catalog numbers of antibodies used in this study are listed: anti-H3K4bbh: PTM-1258, anti-H3K9bbh: PTM-1250, anti-H3K14bbh: PTM-1251, anti-H3K18bbh: PTM-1292, anti-H3K23bbh: PTM-1300, anti-H4K5bbh: PTM-1205, anti-H4K8bbh: PTM-1253, anti-H4K12bbh: PTM-1206, anti-H4K16bbh: PTM-1262, anti-H3: PTM-1001, and anti-H4: PTM-1003.

Co-cocalization analysis

HEK293T cells were transfected with plasmids encoding human sirtuins (SIRT1-7) with C-terminal EGFP using the Lipofectmine 2000 reagent (Invitrogen). After 48 h of transfection, cells were fixed with 4% (w/v) paraformaldehyde in PBS for 10 min, permeabilized with 0.2% Triton X-100 at room temperature for 5 min, and washed with PBS. Nuclei were counterstained with DAPI Fluoromount-G (Southern Biotech, 0100-20). Fluorescent images were taken with a Zeiss710 confocal laser scanning microscope system. Projected images were generated by ZEN 2 lite software (Carl Zeiss).

Subcellular fractionation analysis

HEK293T cells were harvested by centrifugation and washed with PBS. All fractions were extracted for immunoblotting assays using Subcellular Protein Fractionation Kit for Cultured Cells (Thermo Scientific).

Accession codes

The atomic coordinates and structure factors of SIRT3_{118–399}-H3_{6–15}K9bhb, H3_{1–15}K4bhb, and H4_{11–25}K16bhb have been deposited in Protein Data Bank under accession codes 5Z93, 5Z94, and 5ZGC.

Acknowledgements

We thank the Protein Chemistry Facility at the Center for Biomedical Analysis of Tsinghua University for sample analysis. We thank the staff members at beamline BL17U of the Shanghai Synchrotron Radiation Facility and S. Fan at Tsinghua Center for Structural Biology for their assistance in data collection, and the China National Center for Protein Sciences Beijing for providing facility support. This work was supported by grants from the Ministry of Science and Technology of China (2016YFA0500700), the National Natural Science Foundation of China (91753203 and 31725014), and the Tsinghua University Initiative Scientific Research Program to H.L.

Author contributions

H.L. and X.Z. conceived the study; X.Z. designed and performed the experiments under the guidance of H.L. R.C., J.N., S.Y., H.M., and S.Z. helped with the experiments. H.L. and X.Z. wrote the manuscript.

Conflict of interest

The authors declare that they have no conflict of interest.

Publisher's note

Springer Nature remains neutral with regard to jurisdictional claims in published maps and institutional affiliations.

Supplementary Information accompanies the paper at (<https://doi.org/10.1038/s41421-019-0103-0>).

Received: 26 April 2019 Revised: 16 May 2019 Accepted: 20 May 2019

Published online: 09 July 2019

References

- Ruthenburg, A. J., Allis, C. D. & Wysocka, J. Methylation of lysine 4 on histone H3: Intricacy of writing and reading a single epigenetic mark. *Mol. Cell* **25**, 15–30 (2007).
- Chi, P., Allis, C. D. & Wang, G. G. Covalent histone modifications—miswritten, misinterpreted and mis-erased in human cancers. *Nat. Rev. Cancer* **10**, 457–469 (2010).
- Allfrey, V. G., Faulkner, R. & Mirsky, A. E. Acetylation and methylation of histones and their possible role in the regulation of Rna synthesis. *Proc. Natl Acad. Sci. USA* **51**, 786–794 (1964).
- Brownell, J. E. et al. Tetrahymena histone acetyltransferase A: a homolog to yeast Gcn5p linking histone acetylation to gene activation. *Cell* **84**, 843–851 (1996).
- Verdin, E. & Ott, M. 50 years of protein acetylation: from gene regulation to epigenetics, metabolism and beyond. *Nat. Rev. Mol. Cell Biol.* **16**, 258–264 (2015).
- Choudhary, C., Weinert, B. T., Nishida, Y., Verdin, E. & Mann, M. The growing landscape of lysine acetylation links metabolism and cell signalling. *Nat. Rev. Mol. Cell Biol.* **15**, 536–550 (2014).
- Jenuwein, T. & Allis, C. D. Translating the histone code. *Science* **293**, 1074–1080 (2001).
- Jiang, T., Zhou, X., Taghizadeh, K., Dong, M. & Dedon, P. C. N-formylation of lysine in histone proteins as a secondary modification arising from oxidative DNA damage. *Proc. Natl Acad. Sci. USA* **104**, 60–65 (2007).
- Chen, Y. et al. Lysine propionylation and butyrylation are novel post-translational modifications in histones. *Mol. Cell. Proteom.* **6**, 812–819 (2007).
- Goudarzi, A. et al. Dynamic competing histone H4 K5K8 acetylation and butyrylation are hallmarks of highly active gene promoters. *Mol. Cell* **62**, 169–180 (2016).
- Tan, M. J. et al. Identification of 67 histone marks and histone lysine crotonylation as a new type of histone modification. *Cell* **146**, 1015–1027 (2011).
- Xie, Z. Y. et al. Lysine succinylation and lysine malonylation in histones. *Mol. Cell. Proteom.* **11**, 100–107 (2012).
- Tan, M. J. et al. Lysine glutarylation is a protein posttranslational modification regulated by SIRT5. *Cell Metab.* **19**, 605–617 (2014).
- Dai, L. et al. Lysine 2-hydroxyisobutyrylation is a widely distributed active histone mark. *Nat. Chem. Biol.* **10**, 365–370 (2014).
- Xie, Z. et al. Metabolic regulation of gene expression by histone lysine beta-hydroxybutyrylation. *Mol. Cell* **62**, 194–206 (2016).
- Sabari, B. R., Zhang, D., Allis, C. D. & Zhao, Y. M. Metabolic regulation of gene expression through histone acylations. *Nat. Rev. Mol. Cell Biol.* **18**, 90–101 (2017).
- Zhao, S., Zhang, X. & Li, H. Beyond histone acetylation-writing and erasing histone acylations. *Curr. Opin. Struct. Biol.* **53**, 169–177 (2018).
- Newman, J. C. & Verdin, E. beta-Hydroxybutyrate: a signaling metabolite. *Annu. Rev. Nutr.* **37**, 51–76 (2017).
- Jing, H. & Lin, H. N. Sirtuins in epigenetic regulation. *Chem. Rev.* **115**, 2350–2375 (2015).
- Hall, J. A., Dominy, J. E., Lee, Y. & Puigserver, P. The sirtuin family's role in aging and age-associated pathologies. *J. Clin. Invest.* **123**, 973–979 (2013).
- Houtkooper, R. H., Pirinen, E. & Auwerx, J. Sirtuins as regulators of metabolism and healthspan. *Nat. Rev. Mol. Cell Biol.* **13**, 225–238 (2012).
- Feldman, J. L., Baeza, J. & Denu, J. M. Activation of the protein deacetylase SIRT6 by long-chain fatty acids and widespread deacetylation by mammalian sirtuins. *J. Biol. Chem.* **288**, 31350–31356 (2013).
- Bao, X. et al. Identification of 'erasers' for lysine crotonylated histone marks using a chemical proteomics approach. *Elife* **3**, e02999 (2014).
- Anderson, K. A. et al. SIRT4 Is a lysine deacylase that controls leucine metabolism and insulin secretion. *Cell Metab.* **25**, 838 (2017).
- Pannek, M. et al. Crystal structures of the mitochondrial deacylase Sirtuin 4 reveal isoform-specific acyl recognition and regulation features. *Nat. Commun.* **8**, 1513 (2017).
- Du, J. T. et al. Sirt5 is a NAD-dependent protein lysine demalonylase and desuccinylase. *Science* **334**, 806–809 (2011).
- Hirscheby, M. D. & Zhao, Y. M. Metabolic regulation by lysine malonylation, succinylation, and glutarylation. *Mol. Cell. Proteom.* **14**, 2308–2315 (2015).
- Jiang, H. et al. SIRT6 regulates TNF-alpha secretion through hydrolysis of long-chain fatty acyl lysine. *Nature* **496**, 110 (2013).
- Verdin, E., Hirscheby, M. D., Finley, L. W. S. & Haigis, M. C. Sirtuin regulation of mitochondria: energy production, apoptosis, and signaling. *Trends Biochem. Sci.* **35**, 669–675 (2010).

30. Scher, M. B., Vaquero, A. & Reinberg, D. SirT3 is a nuclear NAD(+)-dependent histone deacetylase that translocates to the mitochondria upon cellular stress. *Gene Dev.* **21**, 920–928 (2007).
31. Vaquero, A., Sternglanz, R. & Reinberg, D. NAD+–dependent deacetylation of H4 lysine 16 by class III HDACs. *Oncogene* **26**, 5505–5520 (2007).
32. Sengupta, A. & Haldar, D. Human sirtuin 3 (SIRT3) deacetylates histone H3 lysine 56 to promote nonhomologous end joining repair. *DNA Repair* **61**, 1–16 (2018).
33. Boukouris, A. E., Zervopoulos, S. D. & Michelakis, E. D. Metabolic enzymes moonlighting in the nucleus: metabolic regulation of gene transcription. *Trends Biochem. Sci.* **41**, 712–730 (2016).
34. Borra, M. T., Langer, M. R., Slama, J. T. & Denu, J. M. Substrate specificity and kinetic mechanism of the Sir2 family of NAD(+)-dependent histone/protein deacetylases. *Biochemistry* **43**, 9877–9887 (2004).
35. Jin, L. et al. Crystal structures of human SIRT3 displaying substrate-induced conformational changes. *J. Biol. Chem.* **284**, 24394–24405 (2009).
36. Girdlestone, C. & Hayward, S. The DynDom3D webserver for the analysis of domain movements in multimeric proteins. *J. Comput. Biol.* **23**, 21–26 (2016).
37. Yan, K. et al. Mutations in the chromatin regulator gene BRPF1 cause syndromic intellectual disability and deficient histone acetylation. *Am. J. Hum. Genet.* **100**, 91–104 (2017).
38. Xiong, X. et al. Selective recognition of histone crotonylation by double PHD fingers of MOZ and DPF2. *Nat. Chem. Biol.* **12**, 1111–1118 (2016).
39. Munoz, V. & Serrano, L. Intrinsic secondary structure propensities of the amino-acids, using statistical Phi-Psi matrices—comparison with experimental scales. *Proteins* **20**, 301–311 (1994).
40. Watson, P. J. et al. Insights into the activation mechanism of class I HDAC complexes by inositol phosphates. *Nat. Commun.* **7**, 11262 (2016).
41. Dutta, A., Abmayr, S. M. & Workman, J. L. Diverse activities of histone acylations connect metabolism to chromatin function. *Mol. Cell* **63**, 547–552 (2016).
42. Wakil, S. J. Studies on the fatty acid oxidizing system of animal tissues. IX. Stereospecificity of unsaturated acyl CoA hydase. *Biochim. Biophys. Acta* **19**, 497–504 (1956).
43. Sabari, B. R. et al. Intracellular crotonyl-CoA stimulates transcription through p300-catalyzed histone crotonylation. *Mol. Cell* **58**, 203–215 (2015).
44. Bhedra, P., Jing, H., Wolberger, C. & Lin, H. The substrate specificity of sirtuins. *Annu. Rev. Biochem.* **85**, 405–429 (2016).
45. Smith, B. C., Settles, B., Hallows, W. C., Craven, M. W. & Denu, J. M. SIRT3 substrate specificity determined by peptide arrays and machine learning. *ACS Chem. Biol.* **6**, 146–157 (2011).
46. Rauh, D. et al. An acetylome peptide microarray reveals specificities and deacetylation substrates for all human sirtuin isoforms. *Nat. Commun.* **4**, 2327 (2013).
47. Hebert, A. S. et al. Calorie restriction and SIRT3 trigger global reprogramming of the mitochondrial protein acetylome. *Mol. Cell* **49**, 186–199 (2013).
48. Rardin, M. J. et al. Label-free quantitative proteomics of the lysine acetylome in mitochondria identifies substrates of SIRT3 in metabolic pathways. *Proc. Natl Acad. Sci. USA* **110**, 6601–6606 (2013).
49. Wang, W. W., Zeng, Y., Wu, B., Deiters, A. & Liu, W. R. A chemical biology approach to reveal Sirt6-targeted histone H3 sites in nucleosomes. *ACS Chem. Biol.* **11**, 1973–1981 (2016).
50. Tanabe, K. et al. LC-MS/MS-based quantitative study of the acyl group- and site-selectivity of human sirtuins to acylated nucleosomes. *Sci. Rep.* **8**, 2656 (2018).
51. Watson, P. J., Fairall, L., Santos, G. M. & Schwabe, J. W. R. Structure of HDAC3 bound to co-repressor and inositol tetraphosphate. *Nature* **481**, 335–U114 (2012).
52. Lee, K. K. & Workman, J. L. Histone acetyltransferase complexes: one size doesn't fit all. *Nat. Rev. Mol. Cell Biol.* **8**, 284–295 (2007).
53. Hsu, C. C. et al. Recognition of histone acetylation by the GAS41 YEATS domain promotes H2AZ deposition in non-small cell lung cancer. *Gene Dev.* **32**, 58–69 (2018).
54. Morinieri, J. et al. Cooperative binding of two acetylation marks on a histone tail by a single bromodomain. *Nature* **461**, 664–668 (2009).
55. Flynn, E. M. et al. A subset of human bromodomains recognizes butyryllysine and crotonyllysine histone peptide modifications. *Structure* **23**, 1801–1814 (2015).
56. Otwinowski, Z. & Minor, W. Processing of X-ray diffraction data collected in oscillation mode. *Method Enzymol.* **276**, 307–326 (1997).
57. Vagin, A. & Teplyakov, A. Molecular replacement with MOLREP. *Acta Crystallogr. D* **66**, 22–25 (2010).
58. Adams, P. D. et al. PHENIX: a comprehensive Python-based system for macromolecular structure solution. *Acta Crystallogr. D* **66**, 213–221 (2010).
59. Emsley, P. & Cowtan, K. Coot: model-building tools for molecular graphics. *Acta Crystallogr. D* **60**, 2126–2132 (2004).